Chemical Geology 362 (2013) 82–90

Contents lists available at ScienceDirect

Chemical Geology

journal homepage: www.elsevier.com/locate/chemgeo

Uranium in iron formations and the rise of atmospheric oxygen

C.A. Partin [a,*], S.V. Lalonde [b], N.J. Planavsky [c], A. Bekker [a], O.J. Rouxel [b,d], T.W. Lyons [e], K.O. Konhauser [f]

[a] Dept. of Geological Sciences, University of Manitoba, Winnipeg, Manitoba R3T 2N2, Canada
[b] European Institute for Marine Studies (IUEM), UMR 6538, Technopôle Brest-Iroise, 29280 Plouzané, France
[c] Department of Geology and Geophysics, Yale University, New Haven, CT 06520, USA
[d] Institut Français de Recherche pour l'Exploitation de la Mer (IFREMER), Centre de Brest, 29280 Plouzané, France
[e] Dept. of Earth Sciences, University of California, Riverside, CA 92521, USA
[f] Dept. of Earth and Atmospheric Sciences, University of Alberta, Edmonton, AB T6G 2E3, Canada

ARTICLE INFO

Article history:
Accepted 11 September 2013
Available online 19 September 2013

Keywords:
Atmosphere–ocean oxygenation
Great Oxidation Event
Iron formations
Paleoproterozoic
Geochemical uranium cycle

ABSTRACT

The concept of the Great Oxidation Event (GOE), during which atmospheric oxygen rose precipitously and perhaps to near-modern levels around 2.4–2.1 billion years ago (Ga), has become entrenched in our views on secular atmospheric evolution. Multiple proxies confirm a permanent shift towards more oxygenated conditions at some time near the Archean–Proterozoic boundary. However, it remains unclear precisely when this transition occurred, due in part to the likely temporal variability in those early levels and different sensitivities of the proxies utilized to track atmospheric oxygen partial pressures. Here, we provide a new look at the timing and magnitude of early atmospheric oxygenation through the record of uranium (U) concentrations in iron formations (IF). Just as IF are important archives of the redox state of seawater, concentrations of redox-sensitive U in IF are faithful proxies for oxidative continental weathering and associated delivery of dissolved U to seawater. Our dataset suggests that there was an increase in U redox cycling and transport at ca. 2.47 Ga, just before the permanent loss of mass-independent sedimentary sulfur isotope anomalies traditionally used to define the onset of the GOE. Further, there is significant temporal variability in the IF U record that we propose reflects dynamic Precambrian redox conditions. We provide additional support for earlier suggestions that the GOE was a protracted event marked by vacillating oxygen levels.

1. Introduction

From its inception, the concept of an initial, irreversible rise of atmospheric oxygen beyond some threshold value, the so-called 'Great Oxidation Event' (GOE; Holland, 2002), has been difficult to define in terms of its timing, duration, and magnitude. This remains so despite decades of work, a relationship likely mirroring the complexity of the event. Dick Holland's work has underpinned our basic understanding of the GOE, which was aptly named by him for the dramatic geochemical changes he recognized to be associated with this 'event.' Without question, Dick Holland fundamentally changed our knowledge of oxygenation trends through time; we honor that contribution by continuing to refine those trends. Presently, numerous paleoredox proxies suggest that the first transition from an anoxic to an oxic atmosphere, and the first widespread oxidative weathering of the continents, occurred transiently right at the Archean–Proterozoic boundary at 2.5 Ga (e.g., Anbar et al., 2007; Kump, 2008; Reinhard et al., 2009; Duan et al., 2010; Kendall et al., 2010), and then as a more prominent process by around 2.48 Ga (Konhauser et al., 2011). Atmospheric oxygen concentrations are thought to have reached 1 to 10% of present atmospheric level (PAL), and perhaps much higher, by ca. 2.3–2.1 Ga (Holland, 1994; Bekker et al., 2004; Kump, 2008; Bekker and Holland, 2012). Despite these basic constraints, the exact timing and temporal fabric of the GOE remain poorly constrained. This work strives to better define the first rise in atmospheric O_2 related to the GOE.

Typically, the GOE has been defined as a single event (cf. Holland, 2002) starting with the loss of mass-independent sulfur isotope fractionation (S-MIF) from the sedimentary record between ca. 2.45 and 2.32 Ga (Farquhar et al., 2000; Bekker et al., 2004; Guo et al., 2009). The S-MIF signal is generally attributed to low atmospheric oxygen levels, $<10^{-5}$ PAL according to atmospheric models (Pavlov and Kasting, 2002), or, alternatively, to methane mixing ratios above 3×10^{-5} bars (Zahnle et al., 2006). The GOE might instead be viewed as a more protracted event marked by rising and falling oxygen levels rather than a secular change marked by the loss of S-MIF. We might, therefore, think of the GOE as an interval of time rather than an event, which included earlier stages of continental oxidation tied to the initial rise of atmospheric oxygen before the ultimate loss of S-MIF (e.g., Anbar et al., 2007; Konhauser et al., 2011; Reinhard et al., 2013a).

Given the dynamic geochemical backdrop of the GOE, each paleoredox proxy may offer unique minimum or maximum constraints on atmospheric oxygen level and the redox state of the oceans because of differing redox sensitivities. Accordingly, redox-sensitive elements

* Corresponding author.
E-mail address: camille.partin@umanitoba.ca (C.A. Partin).

0009-2541/$ – see front matter © 2013 Elsevier B.V. All rights reserved.
http://dx.doi.org/10.1016/j.chemgeo.2013.09.005

could have varied in their responses to the rise in atmospheric oxygen. For example, significant U enrichment in shales first occurs in the Timeball Hill and Rooihoogte formations of South Africa (Partin et al., 2013), the units immediately above the Duitschland Formation (Bekker et al., 2004) where the loss of S-MIF is recorded (Bekker et al., 2004; Guo et al., 2009). There is also a shift in the extent of iron isotope variability in sedimentary rocks interpreted to reflect a change in oceanic redox state at around 2.35 Ga (Rouxel et al., 2005; Planavsky et al., 2012b). However, there are also notable stratigraphic Mo and Re enrichments in the much older 2.5 Ga Mount McRae Shale of Western Australia (Anbar et al., 2007), in addition to changes in sedimentary sulfur (Kaufman et al., 2007), nitrogen (Garvin et al., 2009), and molybdenum isotope compositions (Duan et al., 2010) that point to at least mild oxidative weathering conditions during the deposition of this unit, which may have resulted in H_2S-bearing (euxinic) water column conditions with enhanced primary productivity (Reinhard et al., 2009; Raiswell et al., 2011). Similar geochemical observations and conclusions have been made for shallow-water facies of the coeval Klein Naute Formation in the Griqualand West basin of South Africa (Kendall et al., 2010). Furthermore, the U isotope composition of the Mount McRae Shale has been interpreted to be consistent with U mobility at that time, implying oxidative weathering and delivery of U to the oceans (Kendall et al., 2013–in this issue). Partial oxygenation, that is enough oxygen to permit some oxidative continental weathering, could have occurred before the rise of atmospheric oxygen as defined by the loss of S-MIF, or alternatively, continuation of the S-MIF signal through sedimentary recycling after oxygen levels rose above 10^{-5} PAL (Reinhard et al., 2013a). In this scenario, the S-MIF signal could be derived from oxidative weathering of older (Archean) sedimentary sulfides after the 10^{-5} PAL threshold was exceeded (Reinhard et al., 2013a). With this in mind, it is possible that atmospheric oxygen levels were above 10^{-5} PAL for periods from 2.5 to 2.32 Ga despite the persistence of the sedimentary S-MIF signal throughout that period. The coexistence of the S-MIF signal and at least partial oxygenation is evidenced by extensive Cr mobilization at ca. 2.48 Ga (Konhauser et al., 2011), transient terrestrial sulfide oxidation at ca. 2.5 Ga (e.g., Anbar et al., 2007; Reinhard et al., 2009; Duan et al., 2010; Kendall et al., 2010), and perhaps even earlier (Wille et al., 2007; Voegelin et al., 2010) based on Mo isotope systematics in carbonate and shale, and Re abundances in shale (Kendall et al., 2010).

Further complicating the story of Paleoproterozoic redox evolution, several lines of evidence point towards a drop in post-GOE atmospheric oxygen level at Earth's surface. Specifically, the U record of anoxic shales suggests that atmospheric oxygen levels declined around 2.05 Ga (Partin et al., 2013). The sulfate evaporite and S isotope records also indicate a fall in atmospheric–oceanic oxygen levels between 2.1 and 2.0 Ga (Schröder et al., 2008; Bekker and Holland, 2012; Planavsky et al., 2012a).

Despite the emerging view of post-GOE atmospheric oxygen fluctuations, uncertainties remain. We aim to clarify the timing and structure of Earth's first oxygenation by exploring the redox-sensitive nature of U in seawater and its history as recorded by U enrichments in iron formations (IF), which are iron- and silica-rich chemical sediments deposited throughout much of the Precambrian. Because these sediments precipitated directly from seawater, their chemical composition has been widely used as a proxy for ancient seawater composition. For instance, the IF record has been used to decipher first-order trends in the concentrations of Ni and P in Precambrian seawater (Bjerrum and Canfield, 2002; Konhauser et al., 2009; Planavsky et al., 2010). The IF record is particularly well-suited to recording variations in the U content of seawater as the geochemical cycles of U and Fe are closely linked, with the U(VI)/U(IV) and Fe(III)/Fe(II) redox couples being similar in reduction potential (e.g., Barnes and Cochran, 1993; Bruno et al., 1995). Most U in IF is likely to have been derived directly from seawater by adsorption and co-precipitation processes (see 4. Discussion); it is this aspect of IF that confers their ability to track the content of soluble U(VI) in seawater. Utilizing the framework established by the U in shales record (Partin et al., 2013), which provides a high temporal resolution record of the changes in U seawater chemistry and oxidative continental weathering, the IF record provides an opportunity to further explore changes in the U record related to the GOE by bridging the two proxies. While the U concentration of both IF and shales is limited by concentration of U in contemporaneous seawater, each reflects two separate, coexisting sinks that, combined, provide a more complete picture of marine U cycling through time. Additionally, both lithologies are nonuniformly preserved in the geologic record, and therefore, one can be used to fill temporal gaps in the other, e.g., the IF record fills a critical gap in the available 2.45 to 2.32 Ga shale record. Although the two lithologies have notably different depositional styles and temporal distribution, the IF and shale records show remarkably similar trace element histories, reinforcing the view that both lithologies archive changes in seawater composition.

2. Methods

The dataset of iron formation and iron-rich chemical sediments presented here is comprised of both new analyses and a comprehensive literature compilation (see Table 1 for a list of IF units with U data available and Supplementary data Table S1 for sample values). Samples with a high degree of weathering, alteration, metamorphic or diagenetic overprinting were avoided. Specifically, the data were filtered for metamorphic grade (upper greenschist facies or below, as a baseline to maintain a comparable mineralogy between samples), sulfur content (<1%), iron content (5–60%), and compatible mineralogy—in other words, limited to Fe- and Si-rich chemical sediments and excluding sulfides and carbonates. The filtered dataset includes 1315 U concentration values, 591 of which are derived from analysis of bulk powders after digestion, and 724 from laser ablation of polished thin sections; an additional 148 values are included in Table S1 that pass all filter criteria except metamorphic grade (see Fig. 1A). For new data presented here, drill core and hand samples were cleaned and then powdered in an agate mill or processed into thin sections (see Konhauser et al., 2011 for further details). Data were acquired at the University of Alberta using a PerkinElmer Elan6000 Quadrupole Inductively Coupled Plasma Mass Spectrometer (Q-ICP-MS) in solution mode (after heated HF–HNO_3 digestion) or by in-situ laser ablation with a New Wave Research UP-213 laser. Precision was monitored by repeated analyses of international standards BE-N Basalt (CRPG Nancy) in solution mode and NIST glasses SRM 610 and 612 by laser ablation. At the Woods Hole Oceanographic Institution (WHOI) and IFREMER (French Research Institute for Exploitation of the Sea, Brest), samples were sequentially digested in heated HF + HNO_3, *aqua regia*, and 6 N HCl with trace H_2O_2. Data were acquired in solution mode using a ThermoElectron Inc. Element 2 double focusing magnetic sector field ICP-MS and were normalized against repeated analyses of international standards IF-G (CRPG Nancy) and BHVO-1 (USGS). The *in situ* grain-by-grain laser-ablation data (from hematite and magnetite) should give more insight into the U concentrations associated with the iron oxide mineral phase itself, assumed to reflect the vestige of precursor ferric oxyhydroxide minerals (such as ferrihydrite), as opposed to the U concentration of the bulk sample; the data obtained with these two analytical methods provides a useful comparison of mineral-specific U concentrations relative to conventional bulk analysis U concentrations. Precision in U concentration analyses is estimated to be better than 10% for all data. Radioactive decay causes some U and Th to be lost over geological time; U and Th concentrations were corrected for radioactive decay with respect to their host sediment age by assuming that the majority of U is ^{238}U and the majority of Th is ^{232}Th as follows (e.g., Faure, 1986): $[U]_{corrected} = [U]_{measured} \times e^{0.155125 \times Age\ (Ga)}$ and $[Th]_{corrected} = [Th]_{measured} \times e^{0.049475 \times Age\ (Ga)}$. For the oldest samples, corrected U and Th concentrations were 1.8× and 1.2×measured concentrations, respectively.

Table 1
List of IF and associated geological information for units included in this study. Metamorphic grade: A = amphibolite metamorphic grade, G = greenschist metamorphic grade (or lower); IF classification and analysis type: 1-Algoma-type laser-ablation analyses, 2-Algoma-type bulk sample analyses, 3-Superior-type laser-ablation analyses, 4-Superior-type bulk sample analyses, 5-Ironstone laser-ablation analyses, 6-Ironstone bulk sample analyses, 7-Phanerozoic hydrothermal deposits; (last column): LA = laser ablation analysis.

Sample unit	Geographic location	Age	Met. grade	IF classification and analysis type	References for data/geological details
Nuvvuagittuq supracrustal belt	Quebec, Canada	3.8 Ga	A	2	Cates and Mojzsis (2007), Mloszewska et al. (2012), O'Neil et al. (2007)
Isua Greenstone Belt	Greenland	3.75 Ga	A	2	(Bolhar et al., 2004; Dymek and Klein, 1988; Frei and Polat, 2007; bulk analyses, this study; LA analyses, this study)
Panorama Formation, Warrawoona Group	Australia	3.45 Ga	G	2	Bolhar et al. (2005)
Fig Tree Group, Barberton Greenstone Belt	South Africa	3.25 Ga	G	3	(Hofmann, 2005; LA analyses, this study)
Jharkhand–Orissa region IF	India	3.15–3.12 Ga	A	2	Bhattacharya et al. (2007)
Pongola Supergroup	South Africa	2.95 Ga	G	2, 4	(Alexander et al., 2008; bulk analyses, this study)
Bababudan Greenstone Belt	India	2.75 Ga	A	2	Klein and Ladeira (2002)
Carajás IF	Brazil	2.74 Ga	G	3, 4	(Klein and Ladeira, 2002; LA analyses, this study)
Temagami IF	Ontario, Canada	2.74 Ga	G	1, 2	(bulk analyses, this study; LA analyses, this study)
Nemo IF	South Dakota, USA	2.73 Ga	G	4	Frei et al. (2008)
Upper Deloro Assemblage	Ontario, Canada	2.72 Ga	G	2	(bulk analyses, this study)
Eleanor Iron Range		2.70 Ga	G	2	(bulk analyses, this study)
Beardmore Area		2.70 Ga	G	2	(bulk analyses, this study)
Belingwe greenstone belt	Zimbabwe	2.70 Ga	G	2	(bulk analyses, this study)
Soudan Iron Formation	Minnesota, USA	2.70 Ga	G	2	(bulk analyses, this study)
Mary River Group, Baffin Island drill core JD-65	Baffin Island, Canada	2.70 Ga	G	2	(bulk analyses, this study)
Atlantic City IF, South Pass greenstone belt	Wind River Range, Wyoming, USA	2.70 Ga	G	2	Frei et al. (2008)
Marra Mamba IF	Western Australia	2.6 Ga	G	3	(LA analyses, this study)
Benchmark IF	South Dakota, USA	2.52 Ga	G	4	(Frei et al., 2008; bulk analyses, this study)
Penge IF	South Africa	2.48 Ga	G	4	(Bau and Dulski, 1996; bulk analyses, this study)
Dales Gorge Member, Brockman IF	Western Australia	2.48 Ga	G	3, 4	(bulk analyses, LA analyses, this study)
Kuruman IF (and correlative IF in Westerberg and Koegas areas)	South Africa	2.47 Ga	G	3, 4	(Bau and Dulski, 1996; Beukes and Klein, 1990; Horstmann and Hälbich, 1995; Klein and Beukes, 1989; Pickard, 2003; bulk analyses, LA analyses, this study)
Griquatown IF	South Africa	2.47 Ga	G	4	Bau and Dulski (1996), Horstmann and Hälbich (1995)
Joffre Member, Brockman IF	Western Australia	2.46 Ga	G	4	(bulk analyses, this study)
Cauê IF	Brazil	2.43 Ga	G	3, 4	(Klein and Ladeira, 2000; Spier et al., 2007; bulk analyses, LA analyses, this study)
Voelwater Subgroup	Griqualand West, South Africa	2.40 Ga	G	4	Schneiderhan et al. (2006)
Timeball Hill IF	South Africa	2.32 Ga	G	4, 5, 6	(bulk analyses, LA analyses, this study)
Maru IF	Nigeria	2.10 Ga	G	2	Adekoya (1998)
Estes IF	South Dakota, USA	2.06 Ga	G	4	Frei et al. (2008)
Homestake IF	South Dakota, USA	2.0 Ga	G	4	Frei et al. (2008)
Roubaix/Nemo and Pactola Dam area IFs	South Dakota, USA	2.0 Ga	G	4	Frei et al. (2008)
Glen Township Formation IF	Minnesota, USA	1.94 Ga	G	4	(bulk analyses, this study)
Biwabik IF	Minnesota, USA	1.88 Ga	G	4	(bulk analyses, this study)
Rochford IF	South Dakota, USA	1.88 Ga	G	4	Frei et al. (2008)
Vulcan IF	Michigan, USA	1.88 Ga	G	4	(bulk analyses, this study)
Negaunee IF		1.88 Ga	G	3, 4	(bulk analyses, LA analyses, this study)
Ironwood IF	Wisconsin, USA	1.88 Ga	G	4	(bulk analyses, this study)
Gunflint IF	Ontario, Canada	1.88 Ga	G	4	(bulk analyses, this study)
Pecos Greenstone Belt	New Mexico, USA	1.72 Ga	G	4	Slack et al. (2009)
Chuanlinggou Formation IF	China	1.70 Ga	G	6	(bulk analyses, this study)
Weatherly Creek IF, Soldier Cap Group	Australia	1.68 Ga	A	4	Hatton and Davidson (2004)
Freedom Formation, Baraboo district	Wisconsin, USA	1.65 Ga	G	6	(bulk analyses, this study)
Sherwin Formation, Roper Group	Australia	1.40 Ga	G	4	(bulk analyses, this study)
Xiamaling Formation	China	1.40 Ga	G	6	(bulk analyses, this study)
Aok Formation, Shaler supergroup	Northwest Territories, Canada	0.8 Ga	G	6	(bulk analyses, this study)
Mineral Fork Formation	Utah, USA	0.77 Ga	G	4	Young (2002)
Urucum IF	Brazil	0.73 Ga	G	4	Klein and Ladeira (2004)
Rapitan IF	Northwest Territories, Canada	0.71 Ga	G	4	Baldwin et al. (2012), Klein and Beukes (1993)
Yerbal IF	Uruguay	>0.56 Ga	G	3	(LA analyses, this study)
Mt. Windsor subprovince exhalites	Eastern Australia	0.49 Ga	G	7	Davidson et al. (2001)
Sillaoru Formation ironstones	Estonia & Russia	0.48 Ga	G	6	Sturesson et al. (1999)
Jasper beds, Lokken Ophiolite	Norway	0.47 Ga	G	7	Grenne and Slack (2005)
Clinton Ironstone	New York, USA	0.43 Ga	G	6	(bulk analyses, this study)
Hematitic cherts and jaspers, Ural Mountains	Russia	0.39 Ga	G	7	Maslennikov et al. (2012)
Hematitic chert, Iberian pyrite belt	Spain & Portugal	0.35 Ga	G	7	Leistel et al. (1997)
Hydrothermal deposits, Shimanto Supergroup	Japan	0.01 Ga	G	7	Kato et al. (2005)
Hydrothermal deposits	Juan de Fuca Ridge, Pacific Ocean	0.00 Ga	G	7	Hrischeva and Scott (2007)

3. Results

Uranium concentration data, authigenic enrichments, and molar U/Fe ratios from over 50 IF and iron-rich chemical sediments are plotted in Fig. 1. Fig. 1A shows all available U concentration data for samples passing our iron and sulfur filters and classified according to the scheme employed by Konhauser et al. (2011) in their study of Cr enrichment in IF. The defined groups are Algoma-type IF, which are

associated with volcanic successions in greenstone belts, and Superior-type IF, which are found in sedimentary successions deposited on continental shelves of passive margins or in cratonic basins (cf. Bekker et al., 2010). Ironstone refers to both Precambrian granular IF and Phanerozoic ironstones; these deposits show clear evidence of shallow-water deposition, as indicated by their granular texture, cross-bedding, and arrangement in channels. While gradation certainly exists among these classes, they are nonetheless useful for classification of IF and carry important depositional connotations (cf. Bekker et al., 2012). The Phanerozoic hydrothermal group comprises low-temperature iron–silica-rich deposits formed from diffuse seafloor venting and modern hydrothermal plume particles. We consider U enrichments in all these types of iron-rich chemical sediments to be tied to seawater U concentrations, since U is depleted in both seafloor hydrothermal vent fluids and low-temperature submarine hydrothermal springs (e.g., Elderfield and Schultz, 1996).

Post-depositional processes may also modify U enrichments; we consider samples at metamorphic grades greater than greenschist facies (e.g., IF from the Isua greenstone belt of Greenland denoted with a star on Fig. 1A) as less likely to preserve a seawater U signature due to the potential for U remobilization, and, as such, they have been filtered from all other plots (see 2. Methods for a full description of filtering criteria). Furthermore, IF that are directly associated with volcanogenic massive sulfide (VMS) or other mineralization (e.g., the ca. 1.7 Ga Weatherly Creek IF) have not been considered in our dataset. The resulting trend in the IF record appears to track the GOE, consistent with the trends shown by other elements in shales and in IF (Fig. 2).

Elemental data were collected via both conventional bulk analysis and grain-by-grain laser-ablation; the data obtained with these two analytical methods are separated on Fig. 1A. Importantly, there is a discernable and comparable trend in both datasets in the transition from low U values at the Archean–Proterozoic boundary: small and rare enrichments in the ca. 2.47 Ga Kuruman IF of South Africa, higher values in the ca. 2.43 Ga Cauê IF of Brazil (~20 ppm bulk, ~50 ppm grain-by-grain analysis), and a prominent peak in the ca. 2.32 Ga Timeball Hill IF (~40 ppm bulk, ~400 ppm grain-by-grain analysis). The U concentrations associated with the mineral grains are higher than those measured in bulk samples, which is expected due to the close association of U with hematite and magnetite (versus chert and Fe-carbonates that are included in bulk analyses). Nonetheless, we are confident that both analyses identify the same trend in tracking the U content of the Archean and Proterozoic oceans. Lastly, samples passing all filter criteria are plotted in Fig. 1B in terms of absolute U concentrations, as well as concentrations of authigenic U, defined as $U_{auth} = [U] - [Th]/3$ (Wignall and Myers, 1988).

4. Discussion

4.1. Source of U for IF and the oceanic U cycle

Strong correspondence between absolute U concentrations and Th-corrected authigenic U concentrations in the IF record (Fig. 1B) indicates that detrital contamination was generally an unimportant source of U. This is not surprising considering the low concentration of U in the upper continental crust (2.7 ppm; Taylor and McLennan, 1985) relative to that in IF, which reaches up to ~400 ppm and averages 5.4 ppm for samples passing all filters. Accordingly, U enrichment in IF must be derived from seawater and thus tracks the dissolved U content of seawater. The only significant source of dissolved U to seawater is riverine runoff, which in turn, reflects oxidative continental weathering and the conversion of rock-hosted U(IV) to soluble U(VI). Felsic igneous rocks, such as granites or pegmatites, are the dominant source of U, which is hosted primarily in uraninite (Grandstaff, 1976). Accessory minerals, such as zircon, apatite, allanite, and monazite, are also important sources of uranium. A small but variable fraction of the total oceanic U budget is also associated with particulate organic carbon

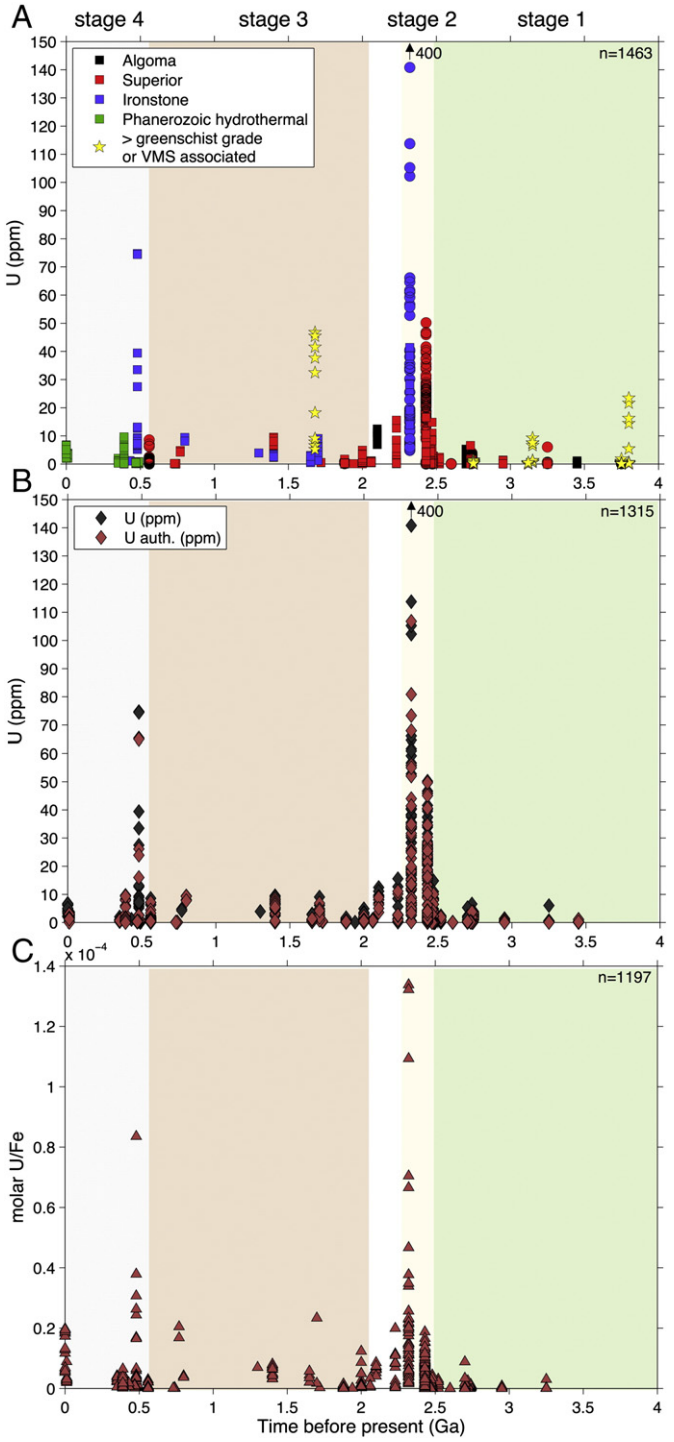

Fig. 1. Secular variations in U content as recorded by IF, reflecting the evolution of the marine U cycle. (A) Data for all samples passing compositional filters, grouped based on iron formation classification (Algoma-type, Superior-type, Ironstone, and Phanerozoic hydrothermal; see 3. Results for more details) as well as analysis type (bulk—squares; laser ablation—circles). Samples failing filters relative to metamorphic grade or association with VMS deposits are highlighted with yellow stars, and are not plotted on subsequent figures. Note that the age of the Hotazel Formation has traditionally been thought to be ca. 2.22 Ga, but could be as old as ca. 2.40 Ga and is plotted with the older age here (see Moore et al., 2012) (B) Absolute U concentrations (gray) and authigenic U concentrations (maroon; corrected for detrital U based on Th content) for samples passing all filters. (C) Molar U/Fe ratios for samples passing all filters.

(e.g., Anderson et al., 1998). A lack of detrital influence on U in our IF dataset is further confirmed by the absence of a correlation with classic detrital indicators (e.g., Al_2O_3 and TiO_2; Supplementary Material

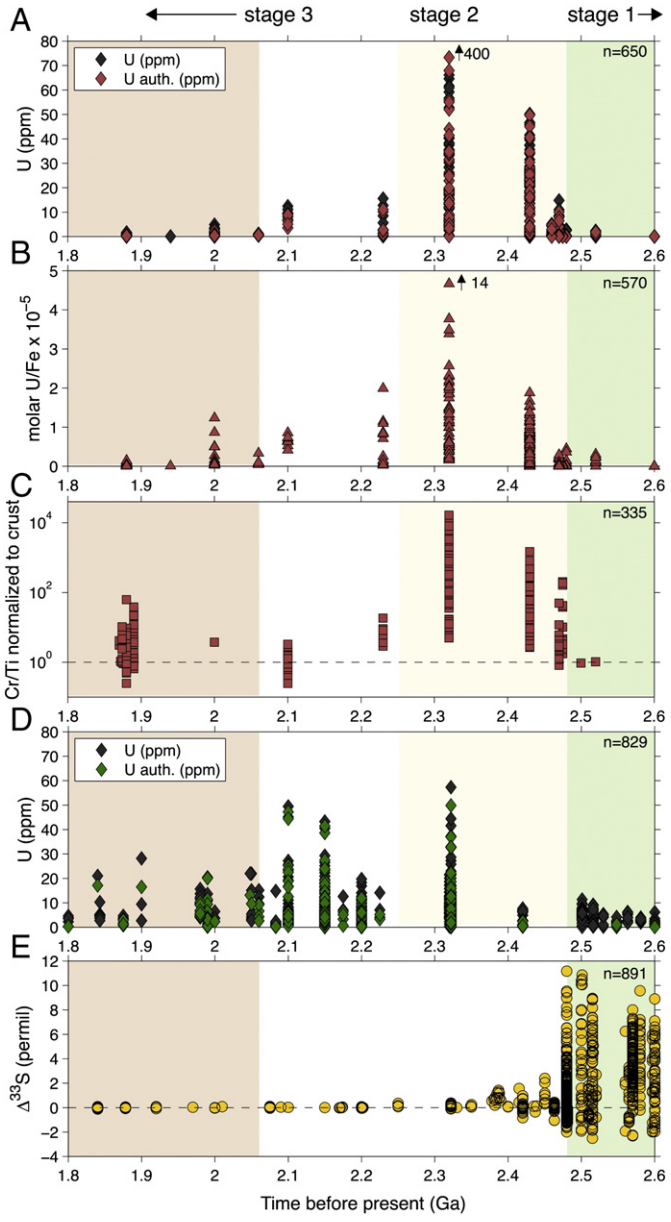

Fig. 2. (A) Secular variations in U content and (B) U/Fe ratio of ca. 2.6 to 1.8 Ga IF together with other relevant surface redox proxies (C–E): (C) Cr/Ti ratios in IF (Konhauser et al., 2011), (D) absolute and authigenic U content of shales (Partin et al., 2013), and (E) sedimentary $\Delta^{33}S$ values (Farquhar et al., 2010; Williford et al., 2011).

Figure S1). Collectively, these relationships tie the sequestration of U into IF to hydrogenous sources (i.e., ocean water column) via U sorption and potentially reduction at the particle-water interface of the IF precursor minerals (e.g., ferric oxyhydroxides). An alternative removal mechanism involves precipitation of U in the sediments rather than scavenging from the water column as observed in modern anoxic basins (Anderson et al., 1989). However, regardless of the specific removal mechanism and locus of enrichment, molar U/Fe ratios in IF (Fig. 1C) generally track absolute and authigenic U concentrations (Fig. 1B), consistent with U sequestration by particle adsorption or surface-catalyzed U reduction from a dissolved U reservoir that has varied significantly over geological time.

Iron formations could have scavenged seawater U(VI) through electrostatic sorption and hydrogen bonding to the surface ligands of iron oxyhydroxides. Laboratory experiments show simultaneous precipitation of Fe(III) and U(VI) from solution, demonstrating significant sorption of uranium on the surface of Fe(III) oxyhydroxides (Bruno et al., 1995). The reduction of U(VI) by ferrous iron requires both a source of soluble Fe(II) and mineral surfaces on which to catalyze the reaction, the products of which are readily taken up by iron oxyhydroxides (Hsi and Langmuir, 1985; Liger et al., 1999). U(VI) has been shown to adsorb onto colloidal magnetite (Missana et al., 2003) and can co-precipitate with hematite and enter the hematite structure (Duff et al., 2002). U(VI) that is co-precipitated or adsorbed onto ferrihydrite may be reduced during the transformation of the iron oxyhydroxide to goethite, which incorporates reduced U into its mineral structure, where it is readily preserved (Boland et al., 2011). The reduction of U(VI) may also be microbially facilitated and generally co-occurs with microbial Fe(III) reduction (Behrends and Van Cappellen, 2005). Regardless, as stated above, it appears that U(VI) reduction requires a particle catalyst (Hsi and Langmuir, 1985; Waite et al., 1994; Liger et al., 1999; Duff et al., 2002; Boland et al., 2011). However, one report has claimed direct reduction of U(VI) by Fe(II) in solution without surface catalysis (Du et al., 2011). Likewise, U has been shown to be elevated on the surface of altered hydrothermal sulfide minerals (Mills et al., 1994) and in sulfidic plume particles on the northern East Pacific Rise (German et al., 2002), reflecting efficient U reduction and removal onto Fe-sulfide particles.

That U is more abundant in our laser-ablation data attests to the association of U with hematite and magnetite, arguing against homogenous nucleation of reduced U mineral phases in the water column and supporting adsorption or reduction at the mineral surface. Finally, analogous to iron, the speciation of U controls its solubility and mobility in seawater and the sequestration of U in ocean sediments. Oxidation and riverine delivery of soluble U are prerequisites to the scavenging and redox reactions between soluble Fe(II) and U(VI) in seawater.

The size of the marine U reservoir tracks the redox evolution of the atmosphere and ocean system (Partin et al., 2013), since the only source of dissolved U to the ocean is via oxidative continental weathering and riverine supply, and the primary removal process from seawater is into anoxic, typically organic-rich marine sediments (Klinkhammer and Palmer, 1991; Dunk et al., 2002). Marine low-temperature hydrothermal systems constitute a smaller sink (Dunk et al., 2002; Mills and Dunk, 2010) via U sequestration into oceanic crust from seawater (German and von Damm, 2003), resulting in net U enrichment in basalt (e.g., Hart and Staudigel, 1982).

Whether by the equilibrium U(VI) surface complexation to ferric oxyhydroxide particles (e.g., Waite et al., 1994) or by the rapid reduction of U(VI) by Fe(II) at the iron oxyhydroxide surface (near-quantitative after ~30 h; Liger et al., 1999), we propose that both U concentrations and molar U/Fe ratios in IF (Fig. 1B and C) should track the evolving dissolved U concentrations of the overlying water column.

4.2. Earth's surface redox evolution based on trends of U in the IF record

Based on the U trends in IF, we have divided our dataset into four stages to further examine Earth's redox evolution (Figs. 1 and 2). Our stage 1 spans from ca. 3.5 Ga, when some of the earliest well-preserved Archean IF were deposited, to just after the Archean–Proterozoic boundary (ca. 2.47 Ga). IF deposited during this time interval are characterized by low U concentrations (<6.6 ppm), with an average value of 0.99 ppm. These concentrations are best explained by limited U mobilization from the continents to the ocean under a dominantly oxygen-poor atmosphere, resulting in a small marine U reservoir, and thus low to negligible concentrations of soluble U in seawater. Overall, low concentrations are consistent with minimal oxidation of U in the Archean atmosphere–ocean system. The U content of seawater at this time is controlled mostly by the small flux of U delivered by continental riverine systems, which, in turn, is limited by the extent to which U is solubilized via oxidative weathering on the continents. The preservation of uraninite (as well as pyrite and siderite) in coarse-grained terrestrial successions is also

consistent with low-oxygen content of the Archean atmosphere (Roscoe and Minter, 1993; Rasmussen and Buick, 1999).

During stage 2, beginning at ca. 2.47 Ga, U concentrations in IF began to ramp up, marking the beginning of the GOE in the broader, protracted sense (Konhauser et al., 2011; Reinhard et al., 2013a). Relatively muted values at ca. 2.48 Ga are followed by several rare but non-trivial enrichments at ca. 2.47 Ga. Further increases are then observed at ca. 2.43 Ga, with the highest U concentrations ever recorded in IF at ca. 2.32 Ga (Figs. 1 and 2A). We interpret this concentration peak to reflect a unique period in the history of Paleoproterozoic surface oxygenation. Though the absolute level of atmospheric oxygen reached is unknown (Kump, 2008), it is plausible that high O_2 levels (>10% PAL) were attained in the Paleoproterozoic (cf. Bekker and Holland, 2012; Partin et al., 2013). The distinction between atmospheric and marine oxygenation is important, as the former governs oxidative weathering and the riverine supply, and the latter mirrors the importance of anoxic, euxinic, and suboxic seafloor sinks. Assuming a modern riverine flux, mass balance considerations indicate that the size of the marine U reservoir is highly sensitive to the extent of oxygenated bottom-waters (Emerson and Huested, 1991; Partin et al., 2013). However, the effect of evolving riverine flux was likely critical during this period of initial growth of the oceanic U reservoir. In this light, the peak in U concentrations in the IF record could be viewed as a maximum in intensity of chemical weathering of the continental crust and U release by widespread oxidative weathering at ca. 2.32 Ga, likely in association with a comparatively small sink area in a relatively oxidized ocean.

It might also be argued that the nearshore, deltaic, depositional setting of the Timeball Hill Formation (cf. Eriksson, 1973; Eriksson and Reczko, 1998; Dorland, 1999), which hosts the most U-enriched IF in our dataset, raises the possibility that some U enrichments could be linked to a strong local continental U flux rather than the global redox state of the Earth's surface system. For instance, it has been suggested that the emergence of an oxygenated atmosphere could have influenced chemical weathering of the continents by generating acidic groundwaters via oxidation of sulfides in the Archean continental crust exposed for the first time at ca. 2.48 Ga to oxidizing weathering (Konhauser et al., 2011), well before the deposition of the Timeball Hill Formation. However, even if the U peak associated with the Timeball Hill IF reflects a local feature at ca. 2.32 Ga, it is difficult to explain the generally increasing U trend during the early Paleoproterozoic as being anything but a global feature given that high U values are found on separate cratons (e.g., Kaapvaal in South Africa, Pilbara in Australia, and São Francisco in Brazil) throughout our stage 2.

For the purpose of the following discussion, we use the original concept of the GOE as a prolonged (>300 Ma) oxidative event (Holland, 2002, 2006). By its sustained nature, the GOE should be marked by redox proxies that converge on a single, overarching oxidative episode for which temporal continuity at >50 Ma timescale is a key factor in distinguishing it semantically from short-term (<10 Ma) transient events that may have preceded it (cf. Anbar et al., 2007) and that were likely important during its incipient stage. Based on the U record of IF, we define GOE initiation just after the Archean–Proterozoic boundary, around 2.47 Ga (Fig. 2; stage 2). Redox-sensitive trace element data in IF point to rising atmospheric oxygen level prior to the disappearance of S-MIF, which continued in the ca. 2.47–2.42 Ga rock record, though the signal was dramatically depressed relative to that between ca. 2.7 and 2.5 Ga (Fig. 2E). The conventional interpretation is that atmospheric pO_2 must have remained below the S-MIF threshold of 10^{-5} PAL (Farquhar et al., 2000; Pavlov and Kasting, 2002) to generate smaller, but non-negligible S-MIF signatures recorded by sediments deposited between ca. 2.47 and 2.42 Ga (Partridge et al., 2008; Williford et al., 2011; Farquhar et al., 2011). However, the exact level of the atmospheric oxygen at which S-MIF would not be produced in the lower atmosphere and would not be recorded in sediments is model-dependent. With this in mind, it is possible that atmospheric oxygen levels were consistent with those required for preservation of S-MIF in the rock record during the 2.47 to 2.42 Ga period and yet at the level sufficient to initiate some level of oxidative continental weathering. Potentially this discrepancy could be resolved if the S-MIF signal prevailed via sedimentary recycling after oxygen rose above the 10^{-5} PAL threshold (Reinhard et al., 2013a). We infer that redox-sensitive trace elements, specifically U, Mo, and Cr, provide a window into the earliest interval of atmospheric oxygen rise that is not reflected by the S-MIF signal, and, through the observed variability in the trace element record, demonstrate a complex fabric of oxygenation pulses throughout the GOE, as broadly defined. The beginning of the GOE is marked by the first notable enrichments above low background levels characteristic of the Archean but more importantly, by the first sign of variability in U content in the IF record, since it should be expected that initial oxygen production would be heavily buffered by sinks for atmospheric oxygen (e.g., oxidative continental weathering, organic matter remineralization, and oxidation of reduced volcanic gases). Oxidative continental weathering in particular constitutes one such sink for which evidence of oxygenation in weathering products should precede sink exhaustion and, in turn, irreversible atmospheric oxygenation. Hence, the timing of GOE initiation as revealed by trace element records might be expected to precede the loss of S-MIF, particularly in the light of the possibility of the persistence of the S-MIF signal via sedimentary recycling, and accordingly, we should look to the earliest continuous signal in the trace element records to guide our definition of GOE initiation.

4.2.1. Comparison with other proxies in the GOE interval

To compare the trends for U to other redox-sensitive proxies that should track the nature, timing, and duration of the GOE, in Fig. 2 we present the U record in IF alongside trends for authigenic Cr enrichment in IF (Konhauser et al., 2011), absolute and authigenic U concentrations in shales (Partin et al., 2013), and the sedimentary record of $\Delta^{33}S$ values (Farquhar et al., 2010, 2011; Williford et al., 2011). These proxies, when combined, paint a coherent picture of the redox evolution of Earth's surface environments after 2.5 Ga. In particular, the records of U and Cr enrichments in IF are remarkably consistent (Fig. 2A–C). There is an increase in Cr enrichments, most likely linked to the oxidation of sulfides in the Archean continental crust at ca. 2.48 Ga (Konhauser et al., 2011), with concentrations further increasing between ca. 2.45 and 2.43 Ga and finally peaking at ca. 2.32 Ga. This trend is consistent with other proxies pointing to complete and persistent atmospheric oxygenation by that time, including highly positive $\delta^{13}C$ values associated with unusually high levels of organic carbon burial beginning around 2.3 Ga (e.g., Karhu and Holland, 1996; Planavsky et al., 2012a), reflecting high rates of O_2 production (Kump et al., 2011). This collective view of the paleoredox records at the Archean–Proterozoic transition supports our assertion that ca. 2.32 Ga was a peak in chemical weathering of the continents and also reflects progressive ocean ventilation during this early interval of the GOE.

Shales and IF are two common lithologies used to trace redox conditions on the early Earth, largely because they are likely to be faithful recorders of past ocean chemistry, and their chemical composition is generally resistant to compromising post-depositional alteration. Redox-sensitive trace element contents in both lithologies are thought to record secular variations in seawater trace element concentrations throughout the Precambrian (as first championed by Holland, 1984). A comparison of U concentration trends for the two hosts (see Fig. 2A and D) appears at first glance to provide contrasting views of surface redox evolution, especially for the period of 2.47–2.43 Ga. The shale record does not show large U enrichments until ca. 2.32 Ga. By contrast, the IF record shows an earlier increase at ca. 2.47 Ga. This discrepancy, however, might be partially an artifact of sample coverage. The IF record (specifically samples from the ca. 2.43 Ga Cauê Formation) fills an important time gap seen in the shale record because of the paucity of analyzed shales with ages between ca. 2.45 and 2.32 Ga. Concentrations of U in IF drop precipitously after ca. 2.32 Ga (Fig. 2), whereas the shale record shows sustained high values from ca. 2.32 to 2.05 Ga, with a sharp

decline thereafter. The difference between the IF and shale U records during this period might reflect increasingly oxidized fluid flow through the sedimentary pile, a phenomenon observed today to promote upwards migration and even release of U from metalliferous sediments after their burial (Mills and Dunk, 2010). The elevated sediment oxygen demand of organic matter-rich sediments, such as black shales, may act to buffer them against such post-depositional migration or loss. This and other possible explanations, such as the presence of strongly depth-dependent water column redox profiles, deserve further attention through multi-proxy examination. Since organic matter-rich shales and IF are non-uniformly preserved throughout geologic time, their geochemical records are limited by the secular availability of the two host lithologies as controlled by their deposition and preservation. The shale record is generally more complete than the IF record, which tends to be episodic, with large IF largely disappearing from the geologic record after ca. 1.85 Ga (cf. Isley and Abbott, 1999; Bekker et al., 2010). Thus, the shale record is often preferred for delineating trends in Earth's redox history. Nevertheless, despite different depositional style and temporal distribution, IF and shale show remarkably similar trace element records, strengthening the validity of archiving changes in seawater composition in both lithologies.

4.2.2. Post-GOE record

The U content of IF during our stage 3, starting at ca. 2.06 Ga, is distinctly lower than that during the GOE (stage 2). In fact, IF deposited at ca. 1.88 Ga have near-crustal U levels. This relationship suggests a lower oxidative capacity at Earth's surface in the late Paleoproterozoic relative to the early Paleoproterozoic, resulting in a smaller seawater U reservoir (Partin et al., 2013). Redox characteristics of the ca. 1.88 Ga atmosphere–ocean system were likely strongly influenced by large hydrothermal fluxes associated with a mantle plume breakout event (Bekker et al., 2010). But, even beyond that geologically short-lived event, the idea of a rise and a subsequent fall in oxygen levels in the Paleoproterozoic atmosphere–ocean system and persistent, low oxygen in the deep ocean throughout the middle Proterozoic is gaining traction through emerging datasets (Scott et al., 2008; Planavsky et al., 2012a; Bekker and Holland, 2012; Reinhard et al., 2013b; Partin et al., 2013) and is herein further corroborated by the record of U in IF. The U content of IF remained low throughout the Meso- and Neoproterozoic. There is, however, a small increase in U enrichment in IF deposited at ca. 715 Ma, suggesting a modest increase in the oceanic U reservoir during the late Neoproterozoic Snowball Earth events. The oceanic U reservoir grew precipitously in the Ediacaran in the aftermath of the Marinoan glaciation (e.g., Sahoo et al., 2012; Partin et al., 2013).

With the Phanerozoic (stage 4) having no true analogs for the depositional conditions that yielded Precambrian IF (i.e., largely anoxic deep waters that allowed for the transport of soluble ferrous iron), it is problematic to use a uniformitarian approach to compare the pre-Phanerozoic record with that of the Phanerozoic. One further complicating factor is that the record of Phanerozoic hydrothermal iron deposits is scarce relative to the pre-Phanerozoic record, so comparison is difficult. However, Phanerozoic hydrothermal iron deposits show only modest U enrichment. The exception is an early Phanerozoic oolitic ironstone bed spanning Russia and Estonia, where unusually high U enrichments (up to 75 ppm) are almost certainly related to extensive carbonate–fluorapatite co-precipitation with this ironstone (up to 35 wt.% P_2O_5). The fact that we do not see large enrichments in the Phanerozoic is perhaps best explained by the transition from more extensive Precambrian iron deposition at ambient seawater temperature to restricted hydrothermally influenced settings during the Phanerozoic. These settings would have depressed the transfer of U into iron-rich sediments as a result of their rapid deposition from concentrated hydrothermal fluids that are inherently U depleted after circulation at depth. Alternatively, low values in Phanerozoic metalliferous hydrothermal deposits and ironstones may be linked to oxic, early-diagenetic alteration resulting in the release of fixed U back into seawater (cf. Dunk and Mills, 2006), as outlined above. Hence, the sink of U with modern hydrothermal sulfide-rich plume particles would be transient, due to the oxic nature of modern seawater. In contrast, the expansive, anoxic deep-waters of the Precambrian oceans should have sequestered U more efficiently due to combined effects of enhanced scavenging onto Fe(II)-rich minerals at or above the seafloor and limited oxidative loss of U during diagenesis.

5. Conclusions

The record of U in IF demonstrates a dramatic shift in the U cycle, including the initial growth of the marine U reservoir associated with the GOE, which started as early as ca. 2.47 Ga. We describe the Paleoproterozoic oxygenation of the atmosphere–ocean system as an interval rather than an event and suggest its initiation is best tracked by a suite of redox-sensitive elements (e.g., U, Mo, Cr, and Re) that signal continental oxidation tied to the initial rise of atmospheric oxygen, prior to the ultimate loss of S-MIF. The earliest GOE interval shows a dynamic transition to more oxygenated conditions, as oxygen production was buffered by oxygen sinks, a state to which redox-sensitive elements in chemical deposits appears to be more sensitive than other redox proxies currently available. The original concept for the initial rise in the atmospheric oxygen level envisaged an oxygenation event around 2.2 to 2.1 Ga (Holland, 1984; Holland et al., 1994; Karhu and Holland, 1996; Holland, 1999). With the recent application of new proxies, better age constraints, and the study of a wider range of lithologies, the concept of the GOE has evolved into a view of a protracted and dynamic sustained period of increasing oxygenation that began much earlier, around 2.47 Ga. This view of the GOE is consistent with other proxies that indicate a long-term increase in atmospheric oxygen content in the early Paleoproterozoic (ca. 2.5 to 2.2 Ga), including Cr enrichment in ca. 2.48 Ga IF (Konhauser et al., 2011), the record of $\Delta^{33}S$ values in ca. 2.47–2.42 Ga shales (Williford et al., 2011; Farquhar et al., 2011), the loss of detrital redox-sensitive minerals from the sedimentary record at ca. 2.4 Ga (Roscoe and Minter, 1993), a spike in U enrichment in ca. 2.32 Ga shales (Partin et al., 2013), a shift in iron content and oxidation state of paleosols at ca. 2.2 Ga (Holland, 1994; Rye and Holland, 1998), significant growth of the marine sulfate reservoir by ca. 2.32 Ga (Planavsky et al., 2012a), and appearance of the first redbeds and shallow-marine sulfate evaporite deposits at ca. 2.32 Ga (Schröder et al., 2008; Farquhar et al., 2011). This impressive collection of redox proxies, converging to roughly agree with the vision of the GOE as laid out by the seminal work of H.D. Holland, testifies to the profound nature of that original vision and highlights the excitement it has inspired today and certainly for generations to follow.

Acknowledgments

The authors wish to thank E. Pecoits and L. Robbins for their contributions towards IF sample collection, analyses, and the compilation of literature data, as well as K. Williford for providing a current compilation of available $\Delta^{33}S$ data. A.B. and K.O.K. were supported by NSERC Discovery Grants. S.V.L. was supported by NSERC PDF award 388101-2010, Europole Mer (Université Européene de Bretagne), and a LabexMER postdoctoral fellowship. N.J.P. was supported by NSF-EAR PDF. T.W.L. was supported by the NASA Exobiology Program and NSF-EAR.

Appendix A. Supplementary data

Supplementary data to this article can be found online at http://dx.doi.org/10.1016/j.chemgeo.2013.09.005.

References

Adekoya, J.A., 1998. The geology and geochemistry of the Maru Banded Iron-Formation, northwestern Nigeria. J. Afr. Earth Sci. 27, 241–257.

Alexander, B.W., Bau, M., Andersson, P., Dulski, P., 2008. Continentally-derived solutes in shallow Archean seawater: rare earth element and Nd isotope evidence in iron formation from the 2.9 Ga Pongola Supergroup, South Africa. Geochim. Cosmochim. Acta 72, 378–394.

Anbar, A.D., Duan, Y., Lyons, T.W., Arnold, G.L., Kendall, B., Creaser, R.A., Kaufman, A.J., Gordon, G.W., Scott, C., Garvin, J., Buick, R., 2007. A whiff of oxygen before the Great Oxidation Event? Science 317, 1903–1906.

Anderson, R.F., Fleisher, M.Q., LeHuray, A.P., 1989. Concentration, oxidation state, and particulate flux of uranium in the Black Sea. Geochim. Cosmochim. Acta 53, 2215–2224.

Anderson, R.F., Kumar, N., Mortlock, R.A., Froelich, P.N., Kubik, P., Dittrich-Hannen, B., Suter, M., 1998. Late-Quaternary changes in productivity of the Southern Ocean. J. Mar. Syst. 17, 497–514.

Baldwin, G.J., Turner, E.C., Kamber, B.S., 2012. A new depositional model for glaciogenic Neoproterozoic iron formation: insights from the chemostratigraphy and basin configuration of the Rapitan iron formation. Can. J. Earth Sci. 49, 455–476.

Barnes, C.E., Cochran, J.K., 1993. Uranium geochemistry in estuarine sediments: controls on removal and release processes. Geochim. Cosmochim. Acta 57, 555–569.

Bau, M., Dulski, P., 1996. Distribution of yttrium and rare-earth elements in the Penge and Kuruman iron-formations, Transvaal Supergroup, South Africa. Precambrian Res. 79, 37–55.

Behrends, T., Van Cappellen, P., 2005. Competition between enzymatic and abiotic reduction of uranium(VI) under iron reducing conditions. Chem. Geol. 220, 315–327.

Bekker, A., Holland, H.D., 2012. Oxygen overshoot and recovery during the early Paleoproterozoic. Earth Planet. Sci. Lett. 317–318, 295–304.

Bekker, A., Holland, H.D., Wang, P.L., Rumble, D., Stein, H.J., Hannah, J.L., Coetzee, L.L., Beukes, N.J., 2004. Dating the rise of atmospheric oxygen. Nature 427, 117–120.

Bekker, A., Slack, J., Planavsky, N., Krapež, B., Hofmann, A., Konhauser, K.O., Rouxel, O.J., 2010. Iron formation: the sedimentary product of a complex interplay among mantle, tectonic, oceanic, and biospheric processes. Econ. Geol. 105, 467–508.

Bekker, A., Krapež, B., Slack, J.F., Planavsky, N., Hofmann, A., Konhauser, K.O., Rouxel, O.J., 2012. Iron formation: the sedimentary product of a complex interplay among mantle, tectonic, oceanic, and biospheric processes—a reply. Econ. Geol. 107, 379–380.

Beukes, N.J., Klein, C., 1990. Geochemistry and sedimentology of a facies transition—from microbanded to granular iron-formation—in the early Proterozoic Transvaal Supergroup, South Africa. Precambrian Res. 47, 99–139.

Bhattacharya, H., Chakraborty, I., Ghosh, K., 2007. Geochemistry of some banded iron-formations of the Archean supracrustals, Jharkhand–Orissa region, India. J. Earth Syst. Sci. 116, 245–259.

Bjerrum, C.J., Canfield, D.E., 2002. Ocean productivity before about 1.9 Gyr ago limited by phosphorus adsorption onto iron oxides. Nature 417, 159–162.

Boland, D.D., Collins, R.N., Payne, T.E., Waite, T.D., 2011. Effect of amorphous Fe(III) oxide transformation on the Fe(II)-mediated reduction of U(VI). Environ. Sci. Technol. 45, 1327–1333.

Bolhar, R., Kamber, B.S., Moorbath, S., Fedo, C.M., Whitehouse, M.J., 2004. Characterisation of early Archaean chemical sediments by trace element signatures. Earth Planet. Sci. Lett. 222, 43–60.

Bolhar, R., Van Kranendonk, M.J., Kamber, B.S., 2005. A trace element study of siderite–jasper banded iron formation in the 3.45 Ga Warrawoona Group, Pilbara Craton—formation from hydrothermal fluids and shallow seawater. Precambrian Res. 137, 93–114.

Bruno, J., De Pablo, J., Duro, L., Figuerola, E., 1995. Experimental study and modeling of the U(VI)-Fe(OH)3 surface precipitation/coprecipitation equilibria. Geochim. Cosmochim. Acta 59, 4113–4123.

Cates, N.L., Mojzsis, S.J., 2007. Pre-3750 Ma supracrustal rocks from the Nuvvuagittuq supracrustal belt, northern Québec. Earth Planet. Sci. Lett. 255, 9–21.

Davidson, G.J., Stolz, A.J., Eggins, S.M., 2001. Geochemical anatomy of silica iron exhalites: evidence for hydrothermal oxyanion cycling in response to vent fluid redox and thermal evolution (Mt. Windsor Subprovince, Australia). Econ. Geol. 96, 1201–1226.

Dorland, H.C., 1999. Paleoproterozoic Laterites, Red Beds and Ironstones of the Pretoria Group with Reference to the History of Atmospheric Oxygen (Master's Thesis). Rand Afrikaans University, Johannesburg, South Africa.

Du, X., Boonchayaanant, B., Wu, W.-M., Fendorf, S., Bargar, J., Criddle, C.S., 2011. Reduction of uranium(VI) by soluble iron(II) conforms with thermodynamic predictions. Environ. Sci. Technol. 45, 4718–4725.

Duan, Y., Anbar, A.D., Arnold, G.L., Lyons, T.W., Gordon, G.W., Kendall, B., 2010. Molybdenum isotope evidence for mild environmental oxygenation before the Great Oxidation Event. Geochim. Cosmochim. Acta 74, 6655–6668.

Duff, M.C., Coughlin, J.U., Hunter, D.B., 2002. Uranium co-precipitation with iron oxide minerals. Geochim. Cosmochim. Acta 66, 3533–3547.

Dunk, R.M., Mills, R.A., 2006. The impact of oxic alteration on plume-derived transition metals in ridge flank sediments from the East Pacific Rise. Mar. Geol. 229, 133–157.

Dunk, R.M., Mills, R.A., Jenkins, W.J., 2002. A reevaluation of the oceanic uranium budget for the Holocene. Chem. Geol. 190, 45–67.

Dymek, R.F., Klein, C., 1988. Chemistry, petrology and origin of banded iron-formation lithologies from the 3800 MA isua supracrustal belt, West Greenland. Precambrian Res. 39, 247–302.

Elderfield, H., Schultz, A., 1996. Mid-ocean ridge hydrothermal fluxes and the chemical composition of the ocean. Annu. Rev. Earth Planet. Sci. 24, 191–224.

Emerson, S.R., Huested, S.S., 1991. Ocean anoxia and the concentrations of molybdenum and vanadium in seawater. Mar. Chem. 34, 177–196.

Eriksson, K.A., 1973. The Timeball Hill Formation—a fossil delta. J. Sediment. Res. 43, 1046–1053.

Eriksson, P.G., Reczko, B.F.F., 1998. Contourites associated with pelagic mudrocks and distal delta-fed turbidites in the Lower Proterozoic Timeball Hill Formation epeiric basin (Transvaal Supergroup), South Africa. Sediment. Geol. 120, 319–335.

Farquhar, J., Bao, H., Thiemens, M., 2000. Atmospheric influence of earth's earliest sulfur cycle. Science 289, 756–758.

Farquhar, J., Wu, N., Canfield, D.E., Oduro, H., 2010. Connections between sulfur cycle evolution, sulfur isotopes, sediments, and base metal sulfide deposits. Econ. Geol. 105, 509–533.

Farquhar, J., Zerkle, A., Bekker, A., 2011. Geological constraints on the origin of oxygenic photosynthesis. Photosynth. Res. 107, 11–36.

Faure, G., 1986. Principles of Isotope Geology, 3rd ed. John Wiley & Sons.

Frei, R., Polat, A., 2007. Source heterogeneity for the major components of ~3.7 Ga Banded Iron Formations (Isua Greenstone Belt, Western Greenland): tracing the nature of interacting water masses in BIF formation. Earth Planet. Sci. Lett. 253, 266–281.

Frei, R., Dahl, P.S., Duke, E.F., Frei, K.M., Hansen, T.R., Frandsson, M.M., Jensen, L.A., 2008. Trace element and isotopic characterization of Neoarchean and Paleoproterozoic iron formations in the Black Hills (South Dakota, USA): assessment of chemical change during 2.9–1.9 Ga deposition bracketing the 2.4–2.2 Ga first rise of atmospheric oxygen. Precambrian Res. 162, 441–474.

Garvin, J., Buick, R., Anbar, A.D., Arnold, G.L., Kaufman, A.J., 2009. Isotopic evidence for an aerobic nitrogen cycle in the latest Archean. Science 323, 1045–1048.

German, C., von Damm, K., 2003. Hydrothermal Processes. In: Elderfield, H. (Ed.), Treatise on Geochemistry: The Oceans and Marine Geochemistry. Elsevier/Pergamon, Oxford, pp. 181–222.

German, C.R., Colley, S., Palmer, M.R., Khripounoff, A., Klinkhammer, G.P., 2002. Hydrothermal plume-particle fluxes at 13°N on the East Pacific Rise. Deep-Sea Res. I Oceanogr. Res. Pap. 49, 1921–1940.

Grandstaff, D.E., 1976. A kinetic study of the dissolution of uraninite. Econ. Geol. 71, 1493–1506.

Grenne, T., Slack, J.F., 2005. Geochemistry of Jasper Beds from the Ordovician Løkken Ophiolite, Norway: origin of proximal and distal siliceous exhalites. Econ. Geol. 100, 1511–1527.

Guo, Q., Strauss, H., Kaufman, A.J., Schröder, S., Gutzmer, J., Wing, B., Baker, M.A., Bekker, A., Jin, Q., Kim, S.-T., Farquhar, J., 2009. Reconstructing Earth's surface oxidation across the Archean–Proterozoic transition. Geology 37, 399–402.

Hart, S.R., Staudigel, H., 1982. The control of alkalies and uranium in seawater by ocean crust alteration. Earth Planet. Sci. Lett. 58, 202–212.

Hatton, O.J., Davidson, G.J., 2004. Soldiers Cap Group iron-formations, Mt Isa Inlier, Australia, as windows into the hydrothermal evolution of a base-metal-bearing Proterozoic rift basin. Aust. J. Earth Sci. 51, 85–108.

Hofmann, A., 2005. The geochemistry of sedimentary rocks from the Fig Tree Group, Barberton greenstone belt: implications for tectonic, hydrothermal and surface processes during mid-Archaean times. Precambrian Res. 143, 23–49.

Holland, H.D., 1984. The Chemical Evolution of the Atmosphere and Oceans. Princeton University Press, Princeton, NJ.

Holland, H.D., 1994. Early Proterozoic atmospheric change. In: Bengston, S. (Ed.), Early Life on Earth, Nobel Symposium No. 84. Columbia University Press, New York, pp. 237–244.

Holland, H.D., 1999. When did the Earth's atmosphere become oxic? A reply. The Geochemical News 20–22.

Holland, H.D., 2002. Volcanic gases, black smokers, and the Great Oxidation Event. Geochim. Cosmochim. Acta 66, 3811–3826.

Holland, H.D., 2006. The oxygenation of the atmosphere and oceans. Philos. Trans. R. Soc. Lond. Ser. B 361, 903–915.

Holland, H.D., Kuo, P.H., Rye, R.O., 1994. O2 and CO2 in the late Archaean and early Proterozoic atmosphere. Mineral. Mag. 58A, 424–425.

Horstmann, U.E., Hälbich, I.W., 1995. Chemical composition of banded iron-formations of the Griqualand West Sequence, Northern Cape Province, South Africa, in comparison with other Precambrian iron formations. Precambrian Res. 72, 109–145.

Hrischeva, E., Scott, S.D., 2007. Geochemistry and morphology of metalliferous sediments and oxyhydroxides from the Endeavour segment, Juan de Fuca Ridge. Geochim. Cosmochim. Acta 71, 3476–3497.

Hsi, C.D., Langmuir, D., 1985. Adsorption of uranyl onto ferric oxyhydroxides: application of the surface complexation site-binding model. Geochim. Cosmochim. Acta 49, 1931–1941.

Isley, A.E., Abbott, D.H., 1999. Plume-related mafic volcanism and the deposition of banded iron formation. J. Geophys. Res. 104, 15461–15477.

Karhu, J.A., Holland, H.D., 1996. Carbon isotopes and the rise of atmospheric oxygen. Geology 24, 867–870.

Kato, Y., Fujinaga, K., Suzuki, K., 2005. Major and trace element geochemistry and Os isotopic composition of metalliferous umbers from the Late Cretaceous Japanese accretionary complex. Geochem. Geophys. Geosyst. 6, Q07004.

Kaufman, A.J., Johnston, D.T., Farquhar, J., Masterson, A.L., Lyons, T.W., Bates, S., Anbar, A.D., Arnold, G.L., Garvin, J., Buick, R., 2007. Late Archean biospheric oxygenation and atmospheric evolution. Science 317, 1900–1903.

Kendall, B., Reinhard, C.T., Lyons, T.W., Kaufman, A.J., Poulton, S.W., Anbar, A.D., 2010. Pervasive oxygenation along late Archaean ocean margins. Nat. Geosci. 3, 647–652.

Kendall, B., Brennecka, G.A., Weyer, S., Anbar, A.D., 2013. Uranium isotope fractionation suggests oxidative uranium mobilization at 2.50 Ga. Chem. Geol. 362, 105–114 (in this issue).

Klein, C., Beukes, N.J., 1989. Geochemistry and sedimentology of a facies transition from limestone to iron-formation deposition in the early Proterozoic Transvaal Supergroup, South Africa. Econ. Geol. 84, 1733–1774.

Klein, C., Beukes, N.J., 1993. Sedimentology and geochemistry of the glaciogenic late Proterozoic Rapitan Iron-Formation in Canada. Econ. Geol. 88, 542–565.

Klein, C., Ladeira, E.A., 2000. Geochemistry and petrology of some proterozoic banded iron-formations of the Quadrilátero Ferrífero, Minas Gerais, Brazil. Econ. Geol. 95, 405–427.

Klein, C., Ladeira, E.A., 2002. Petrography and geochemistry of the least altered banded iron-formation of the Archean Carajás Formation, nothern Brazil. Econ. Geol. 97, 643–651.

Klein, C., Ladeira, E.A., 2004. Geochemistry and mineralogy of Neoproterozoic banded iron-formations and some selected, siliceous manganese formations from the Urucum district, Mato Grosso Do Sul, Brazil. Econ. Geol. 99, 1233–1244.

Klinkhammer, G., Palmer, M., 1991. Uranium in the oceans—where it goes and why. Geochim. Cosmochim. Acta 55, 1799–1806.
Konhauser, K.O., Pecoits, E., Lalonde, S.V., Papineau, D., Nisbet, E.G., Barley, M.E., Arndt, N.T., Zahnle, K., Kamber, B.S., 2009. Oceanic nickel depletion and a methanogen famine before the Great Oxidation Event. Nature 458, 750–753.
Konhauser, K.O., Lalonde, S.V., Planavsky, N.J., Pecoits, E., Lyons, T.W., Mojzsis, S.J., Rouxel, O.J., Barley, M.E., Rosiere, C., Fralick, P.W., Kump, L.R., Bekker, A., 2011. Aerobic bacterial pyrite oxidation and acid rock drainage during the Great Oxidation Event. Nature 478, 369–373.
Kump, L.R., 2008. The rise of atmospheric oxygen. Nature 451, 277–278.
Kump, L.R., Junium, C., Arthur, M.A., Brasier, A., Fallick, A., Melezhik, V., Lepland, A., CČrne, A.E., Luo, G., 2011. Isotopic evidence for massive oxidation of organic matter following the Great Oxidation Event. Science 334, 1694–1696.
Leistel, J.M., Marcoux, E., Deschamps, Y., 1997. Chert in the Iberian Pyrite Belt. Miner. Deposita 33, 59–81.
Liger, E., Charlet, L., Van Cappellen, P., 1999. Surface catalysis of uranium(VI) reduction by iron(II). Geochim. Cosmochim. Acta 63, 2939–2955.
Maslennikov, V.V., Ayupova, N.R., Herrington, R.J., Danyushevskiy, L.V., Large, R.R., 2012. Ferruginous and manganiferous haloes around massive sulphide deposits of the Urals. Ore Geol. Rev. 47, 5–41.
Mills, R.A., Dunk, R.M., 2010. Tracing low-temperature fluid flow on ridge flanks with sedimentary uranium distribution. Geochem. Geophys. Geosyst. 11, Q08009.
Mills, R.A., Thomson, J., Elderfield, H., Hinton, R.W., Hyslop, E., 1994. Uranium enrichment in metalliferous sediments from the Mid-Atlantic Ridge. Earth Planet. Sci. Lett. 124, 35–47.
Missana, T., García-Gutiérrez, M., Fernńdez, V., 2003. Uranium (VI) sorption on colloidal magnetite under anoxic environment: experimental study and surface complexation modelling. Geochim. Cosmochim. Acta 67, 2543–2550.
Mloszewska, A.M., Pecoits, E., Cates, N.L., Mojzsis, S.J., O'Neil, J., Robbins, L.J., Konhauser, K.O., 2012. The composition of Earth's oldest iron formations: the Nuvvuagittuq Supracrustal Belt (Québec, Canada). Earth Planet. Sci. Lett. 317–318, 331–342.
Moore, J.M., Polteau, S., Armstrong, R.A., Corfu, F., Tsikos, H., 2012. The age and correlation of the Postmasburg Group, southern Africa: onstraints from detrital zircon grains. J. Afr. Earth Sci. 64, 9–19.
O'Neil, J., Maurice, C., Stevenson, R.K., Larocque, J., Cloquet, C., David, J., Francis, D., 2007. The geology of the 3.8 Ga Nuvvuagittuq (Porpoise Cove) Greenstone Belt, Northeastern Superior Province, Canada. In: van Kranendonk, M.J., Smithies, R.H., Bennett, V.C. (Eds.), Developments in Precambrian Geology. Elsevier, pp. 219–250.
Partin, C.A., Bekker, A., Planavsky, N.J., Scott, C.T., Gill, B.C., Li, C., Podkovyrov, V., Maslov, A., Konhauser, K.O., Lalonde, S.V., Love, G.D., Poulton, S.W., Lyons, T.W., 2013. Large-scale fluctuations in Precambrian atmospheric and oceanic oxygen levels from the record of U in shales. Earth Planet. Sci. Lett. 369–370, 284–293.
Partridge, M.A., Golding, S.D., Baublys, K.A., Young, E., 2008. Pyrite paragenesis and multiple sulfur isotope distribution in late Archean and early Paleoproterozoic Hamersley Basin sediments. Earth Planet. Sci. Lett. 272, 41–49.
Pavlov, A.A., Kasting, J.F., 2002. Mass-independent fractionation of sulfur isotopes in Archean sediments: strong evidence for an anoxic Archean atmosphere. Astrobiology 2, 27–41.
Pickard, A.L., 2003. SHRIMP U–Pb zircon ages for the Palaeoproterozoic Kuruman Iron Formation, Northern Cape Province, South Africa: evidence for simultaneous BIF deposition on Kaapvaal and Pilbara Cratons. Precambrian Res. 125, 275–315.
Planavsky, N., Rouxel, O., Bekker, A., Lalonde, S.V., Konhauser, K.O., Reinhard, C.T., Lyons, T.W., 2010. The evolution of the marine phosphate reservoir. Nature 467, 1088–1090.
Planavsky, N.J., Bekker, A., Hofmann, A., Owens, J.D., Lyons, T.W., 2012a. Sulfur record of rising and falling marine oxygen and sulfate levels during the Lomagundi event. PNAS 209, 18300–18305.
Planavsky, N.J., Rouxel, O.J., Bekker, A., Hofmann, A., Little, C.T.S., Lyons, T.W., 2012b. Iron isotope composition of some Archean and Proterozoic iron formations. Geochim. Cosmochim. Acta 80, 158–169.
Raiswell, R., Reinhard, C.T., Derkowski, A., Owens, J., Bottrell, S.H., Anbar, A.D., Lyons, T.W., 2011. Formation of syngenetic and early diagenetic iron minerals in the late Archean Mt. McRae Shale, Hamersley Basin, Australia: new insights on the patterns, controls and paleoenvironmental implications of authigenic mineral formation. Geochim. Cosmochim. Acta 75, 1072–1087.
Rasmussen, B., Buick, R., 1999. Redox state of the Archean atmosphere: evidence from detrital heavy minerals in ca. 3250–2750 Ma sandstones from the Pilbara Craton, Australia. Geology 27, 115–118.
Reinhard, C.T., Raiswell, R., Scott, C., Anbar, A.D., Lyons, T.W., 2009. A late Archean sulfidic sea stimulated by early oxidative weathering of the continents. Science 326, 713–716.
Reinhard, C.T., Planavsky, N.J., Lyons, T.W., 2013a. Long-term sedimentary recycling of rare sulphur isotope anomalies. Nature 497, 100–103.
Reinhard, C.T., Planavsky, N.J., Robbins, L.J., Partin, C.A., Gill, B.C., Lalonde, S.V., Bekker, A., Konhauser, K.O., Lyons, T.W., 2013b. Proterozoic ocean redox and biogeochemical stasis. PNAS 110, 5357–5362.
Roscoe, S.M., Minter, W.E.L., 1993. Pyritic paleoplacer gold and uranium deposits. Mineral Deposit Modeling, Geological Association of Canada Special Paper 40. Geological Association of Canada, Toronto, pp. 103–124.
Rouxel, O.J., Bekker, A., Edwards, K.J., 2005. Iron isotope constraints on the Archean and Paleoproterozoic ocean redox state. Science 307, 1088–1091.
Rye, R., Holland, H.D., 1998. Paleosols and the evolution of atmospheric oxygen: a critical review. Am. J. Sci. 298, 621–672.
Sahoo, S.K., Planavsky, N.J., Kendall, B., Wang, X., Shi, X., Scott, C., Anbar, A.D., Lyons, T.W., Jiang, G., 2012. Ocean oxygenation in the wake of the Marinoan glaciation. Nature 489, 546–549.
Schneiderhan, E.A., Gutzmer, J., Strauss, H., Mezger, K., Beukes, N.J., 2006. The chemostratigraphy of a Paleoproterozoic MnF–BIF succession—the Voëlwater Subgroup of the Transvaal Supergroup in Griqualand West, South Africa. S. Afr. J. Geol. 109, 63–80.
Schröder, S., Bekker, A., Beukes, N.J., Strauss, H., Van Niekerk, H.S., 2008. Rise in seawater sulphate concentration associated with the Paleoproterozoic positive carbon isotope excursion: evidence from sulphate evaporites in the ~ 2.2–2.1 Gyr shallow-marine Lucknow Formation, South Africa. Terra Nova 20, 108–117.
Scott, C., Lyons, T.W., Bekker, A., Shen, Y., Poulton, S.W., Chu, X., Anbar, A.D., 2008. Tracing the stepwise oxygenation of the Proterozoic ocean. Nature 452, 456–459.
Slack, J.F., Grenne, T., Bekker, A., 2009. Seafloor-hydrothermal Si–Fe–Mn exhalites in the Pecos greenstone belt, New Mexico, and the redox state of ca. 1720 Ma deep seawater. Geosphere 5, 302–314.
Spier, C.A., de Oliveira, S.M.B., Sial, A.N., Rios, F.J., 2007. Geochemistry and genesis of the banded iron formations of the Cauê Formation, Quadrilátero Ferrífero, Minas Gerais, Brazil. Precambrian Res. 152, 170–206.
Sturesson, U., Dronov, A., Saadre, T., 1999. Lower Ordovician iron ooids and associated oolitic clays in Russia and Estonia: a clue to the origin of iron oolites? Sediment. Geol. 123, 63–80.
Taylor, S.R., McLennan, S.M., 1985. The Continental Crust: its Composition and Evolution. Blackwell Scientific Pub, Oxford.
Voegelin, A.R., Nägler, T.F., Beukes, N.J., Lacassie, J.P., 2010. Molybdenum isotopes in late Archean carbonate rocks: implications for early Earth oxygenation. Precambrian Res. 182, 70–82.
Waite, T.D., Davis, J.A., Payne, T.E., Waychunas, G.A., Xu, N., 1994. Uranium(VI) adsorption to ferrihydrite: application of a surface complexation model. Geochim. Cosmochim. Acta 58, 5465–5478.
Wignall, P.B., Myers, K.J., 1988. Interpreting benthic oxygen levels in mudrocks: a new approach. Geology 16, 452–455.
Wille, M., Kramers, J.D., Nägler, T.F., Beukes, N.J., Schröder, S., Meisel, T., Lacassie, J.P., Voegelin, A.R., 2007. Evidence for a gradual rise of oxygen between 2.6 and 2.5 Ga from Mo isotopes and Re-PGE signatures in shales. Geochim. Cosmochim. Acta 71, 2417–2435.
Williford, K.H., Van Kranendonk, M.J., Ushikubo, T., Kozdon, R., Valley, J.W., 2011. Constraining atmospheric oxygen and seawater sulfate concentrations during Paleoproterozoic glaciation: in situ sulfur three-isotope microanalysis of pyrite from the Turee Creek Group, Western Australia. Geochim. Cosmochim. Acta 75, 5686–5705.
Young, G.M., 2002. Geochemical investigation of a Neoproterozoic glacial unit: the Mineral Fork Formation in the Wasatch Range, Utah. Geol. Soc. Am. Bull. 114, 387–399.
Zahnle, K., Claire, M., Catling, D., 2006. The loss of mass-independent fractionation in sulfur due to a Palaeoproterozoic collapse of atmospheric methane. Geobiology 4, 271–283.